Pulsed laser deposited and sulfurized Cu2ZnSnS4 thin film for efficient solar cell

Ju-Guang Hu, Tong Wu, Muhammad Ishaq, Umar Farooq, Shuo Chen, Zhuang-Hao Zheng, Zheng-Hua Su, Xiao-Dong Lin, Ping Fan, Hongli Ma, et al.

▶ **To cite this version:**

Ju-Guang Hu, Tong Wu, Muhammad Ishaq, Umar Farooq, Shuo Chen, et al.. Pulsed laser deposited and sulfurized Cu2ZnSnS4 thin film for efficient solar cell. Solar Energy Materials and Solar Cells, 2021, 233, pp.111383. 10.1016/j.solmat.2021.111383 . hal-03414165

HAL Id: hal-03414165

https://univ-rennes.hal.science/hal-03414165v1

Submitted on 15 Jun 2023

HAL is a multi-disciplinary open access archive for the deposit and dissemination of scientific research documents, whether they are published or not. The documents may come from teaching and research institutions in France or abroad, or from public or private research centers.

L'archive ouverte pluridisciplinaire **HAL**, est destinée au dépôt et à la diffusion de documents scientifiques de niveau recherche, publiés ou non, émanant des établissements d'enseignement et de recherche français ou étrangers, des laboratoires publics ou privés.

Pulsed Laser Deposited and Sulfurized Cu_2ZnSnS_4 Thin Film for efficient solar cell

Ju-Guang Hu[1], Tong Wu[1], Muhammad Ishaq[1], Umar Farooq[1], Shuo Chen[1], Zhuang-Hao Zheng[1], Zheng-Hua Su[1], Xiao-Dong Lin[1], Ping Fan[1], Hong-Li Ma[2], Xiang-Hua Zhang[2], Guang-Xing Liang*[1]

[1] *Shenzhen Key Laboratory of Advanced Thin Films and Applications, Key Laboratory of Optoelectronic Devices and Systems, College of Physics and Optoelectronic Engineering, Shenzhen University, Shenzhen, 518060, P. R. China*

[2] *Univ Rennes, CNRS, ISCR (Institut des Sciences Chimiques de Rennes) UMR 6226, Rennes, F-35000, France*

*Corresponding author Email: lgx@szu.edu.cn (Prof. Liang)

Abstract

Kesterite quaternary material Cu_2ZnSnS_4, (CZTS)-based thin-film solar cells have attracted intensive attention owing to their earth-abundant nature, stable thermodynamic structure, and large potential for high power conversion efficiency (PCE) defined by their suitable optoelectronic properties. As a widely used thin film preparation method, pulsed laser deposition (PLD) has not been fully studied in CZTS thin-film solar cell. Herein, a promising route based on PLD from a quaternary target and post-sulphuration for CZTS thin film was achieved. Through systematical investigation and optimization of substrate temperature, laser pulse energy, and sulfurization temperature, the CZTS thin films showed single kesterite structure, high (112) orientation, and dense polycrystalline grains with controlled composition. The CZTS thin-film solar cell exhibited a record PCE of 6.62%, the highest reported value when using pulsed laser deposited and sulfurized process, due to its lower series resistance, reduced grain boundary effects, superior interface quality, and a suitable depletion width. This research offers a facile and robust preparation method for CZTS films with enhanced photovoltaic properties and increased efficiency.

Keywords: CZTS; thin film; pulsed laser deposition; solar cell

Introduction

Thin-film solar cells provide an opportunity to reduce the cost of converting solar energy into electricity by replacing expensive and heavy silicon crystal solar cells, thus reducing the total cost of photovoltaic modules by more than 50%.[1] Although solar cells based on chalcopyrite (CIGS) and zinc blende (CdTe) structures have achieved a power conversion efficiency (PCE) of more than 20%,[2] scientific researchers are still trying to find more reliable alternative materials due to the scarcity of indium and the toxicity of Cd. Kesterite-quaternary material Cu_2ZnSnS_4 (CZTS)-based solar cells have become an admirable substitute and the most attractive absorber material on because of their excellent performance, benefitting from non-toxic and earth-abundant elements. CZTS is a p-type semiconductor with a bandgap of 1.5 eV and a high absorption coefficient ($> 10^4$ cm $^{-1}$). [3, 4] Thus, a micron-level film could absorb almost all photons with energy greater than the bandgap. However, the current records of CZTSSe and pure sulfide CZTS are 12.6% and 11.1%, [5, 6] respectively, lower than CIGS and the theoretically predicted efficiency (28%).[7]

Thus, searching for alternative approaches (such as thermal-evaporation, [8-10] sputtering, [11-14] and solution method,[15, 16]) is encouraged for the synthesis of CZTS film to obtain solar cells with increased efficiency. Nowadays, while much progress has been made in scaling co-evaporation for production, this technique for CZTS thin film has several disadvantages, such as films uniformity, difficulty of composition matching by simultaneous control of different evaporation sources, waste materials, possible poor device performance, and repeatability. In the recent work, solution-processed $Cu_2ZnCdSnS_4$ solar cells with a record efficiency of 12.6% in pure sulfide-based kesterite thin-film solar cells were achieved.[15] A decent efficiency of 9.3% for CZTS thin-film solar cell prepared by quaternary target sputtering was obtained.[17] As known, the solution method inevitably introduces different impurities to the material. The reproducibility of vacuum a quaternary target sputtering method is low in terms of composition control. With the rapid development of laser technology, pulsed laser deposition (PLD) as a vacuum physical method has great advantages, and it is widely used in the preparation of complex thin-film materials (especially oxides, nitrides, and

amorphous materials).[18, 19] Its main advantages are as follows: 1. easily obtainable desired stoichiometric ratio of the multi-component film, 2. high deposition rate and low substrate temperature requirement, 3. arbitrarily adjustable parameters with no restriction on the type of target material, 4. ease of preparation of various film materials. During PLD process, a focused high-energy pulsed ultraviolet laser beam bombards the surface of the target material, and sputters from the surface of the target material through phonon interaction to generate gaseous ions to form a plasma plume, which usually comprises ions, neutral atoms or clusters of atoms, and molecules. Plume deposits a film on the substrate held a few centimeters away from the target. Thus, the kinetic energy of the plasma plume and the substrate temperature are sensitive parameters for film formation. CZTS thin-film solar cell fabricated via PLD was first demonstrated by Moriya et al. in 2007, [20, 21] establishing a PCE of 1.74%. Jin et.al. [22] used quaternary oxide target fabricated precursors, performed high-temperature annealing in the presence of H_2S and N_2, and obtained a PCE of 4.94%. Gansukh and his co-workers recently obtained the record PCE (5.4%) for PLD-processed CZTS thin-film solar cells by using oxide precursors.[23] They prepared the precursor through oxide route to solve the volatilization problem of Sn_xS_y in high-temperature annealing condition, and improved the film morphology and device performance. However, for CZTS films sulfurized through oxide precursor, the replacement of O with S may partly consume the driving energy of crystallization, leading to reduced grain growth process.[22] Furthermore, the difference of ionic radius between O and S could lead to considerable lattice expansion, weakening the adhesion on Mo back contact. This phenomenon may lead to high surface roughness, cracks, and irregularities at the absorber/MoS interface, thus restricting the improvement of open-circuit voltage (V_{OC}) and PCE.

In this work, a facile and robust preparation method based on PLD from a quaternary target and post-sulphuration for CZTS thin films was reported. The effect of substrate temperature, laser pulse energy, and sulfurization temperature on the microstructure, composition, and physical properties was discussed in conjunction with the desirable grain structures and purity of kesterite phase for enhanced photovoltaic performance.

Experimental detail

Materials and device fabrication

4 × 4 cm^2 soda-lime glass (SLG) substrate was ultrasonically cleaned in acetone, ethyl alcohol, deionized water for 5 min each, and dried with heating table. Then, a Mo bilayer was deposited by DC magnetron sputtering on the cleaned SLG. The first layer was 200 nm thick, and it was deposited at 100 W DC sputtering power for 20 min. The second layer was 300 nm thick deposited at 250 W sputtering power for 30 min. The working pressure of the magnetron sputtering was under 8 × 10^{-4} Pa. Precursors were deposited with PLD equipment under high vacuum condition (5 × 10^{-4} Pa), as depicted in Figure 1a. The KrF excimer laser (PLD-30, Shenzhen Shengfang Technology Co, Ltd, China) beam (248 nm wavelength, 7 ns pulse-width and 10 Hz pulse repetition rate) was focused onto a sintered target with overall CZTS stoichiometry (5 cm diameter, and Cu:Zn:Sn:S =24:15:12:49) at a spot size of 7 mm^2. The precursors were deposited for 60 min with three different laser energies: i) 50 mJ, ii) 150 mJ, and iii) 250 mJ, and four different substrate temperatures as follows: i) 100 °C, ii) 200 °C, iii) 300 °C, and iii)400 °C. To confirm the composition uniformity of 4 × 4 cm^2 precursor film, the scanning laser aimed at the CZTS target with 20 mm/s and the sample kept rotating with 10 rounds/min. The precursor film was uniform visually in colour in Figure S1 (a) and the thickness of as-deposited precursor film was about 1.3 μm, detected by cross-section SEM images in Figure S1 (b). For post-sulfurization, 0.2 g of highly pure sulfur powder (99.999%) and the as-deposited CZTS thin films were separately placed (25 cm apart) in a double-chamber vacuum tubular furnace (60 mm diameter) (Figure 1b). The chambers were evacuated using a mechanical pump, and argon gas was introduced to thoroughly purge the chambers for 3 times prior to sulfurization, then the pressure in the closed cavity was maintained at 0.03 MPa. The precursor thin films were sulfurized by maintaining the sulfur source zone at 220 °C (achieving the aimed temperature in 30 min and kept for 10 min), and the sample zone at 590 °C – 610 °C, then cooling down naturally with the furnace. Temperature change curve of post-sulfurization process was presented in Figure S2.

The n-type cadmium sulfide (CdS) buffer layer (50 nm thick) was deposited on

sulfurized samples via chemical bath deposition (CBD). The sample is attached to the inner wall of a square quartz cup, later add the solution which contained deionized water (140 mL), $CdSO_4$ (0.015 M, 20 mL), thiourea (0.75 M, 20 mL), and ammonia (14.8 M, 22 mL) in turn. The CBD process was kept at 80 °C for 9 min (Figure 1c). An additional CZTS/CdS heterojunction heat treatment at 250 °C for 10 min in argon atmosphere was designed to induce elemental Cd inter-diffusion and optimize the energy band alignment (Figure 1d). Afterwards, a 400 nm window layer of indium tin oxide (ITO) with a sheet resistance around 18 Ω/sq was deposited by RF magnetron sputtering at 120 W, under a pressure of 0.4 Pa and a flow rate of 30 sccm for argon and oxygen gas (Figure 1e). Finally, Ag electrodes were thermally evaporated on the top of the ITO to obtain the completed the device architecture. Solar cell devices of 0.15 cm^2 were defined by mechanical scribing. A schematic of the CZTS thin-film solar cell with the substrate structure of Mo/CZTS/CdS/ITO/Ag is shown in Figure 1f. A notable detail that the solar cell devices were not coated with MgF_2 as an anti-reflective coating to increase current.

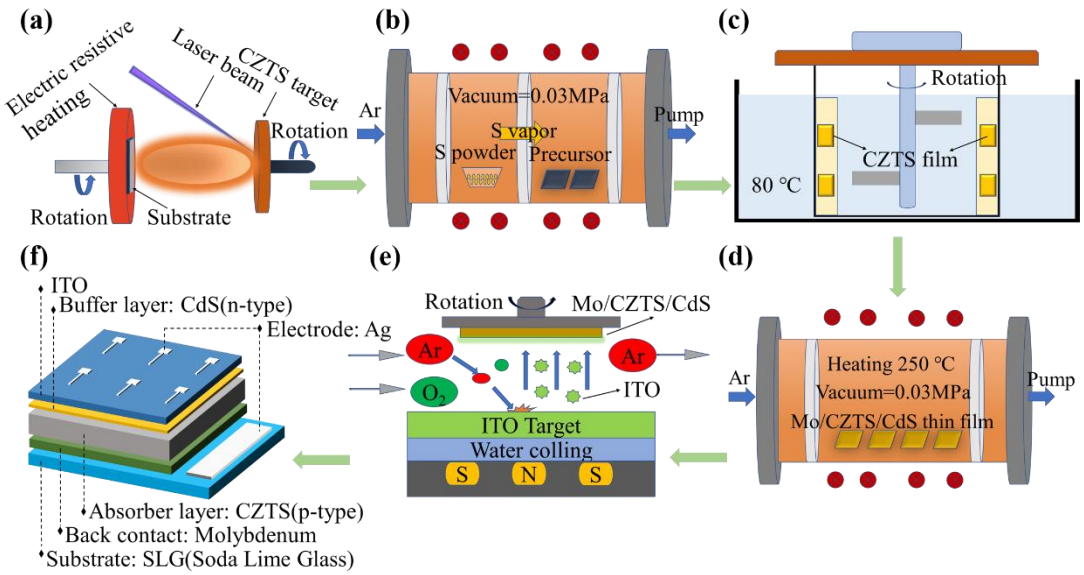

Figure 1. Schematic illustration of the preparation process of the Cu_2ZnSnS_4 thin film solar cell. (a) CZTS precursor thin film deposition by PLD, (b) post-sulfurization heat treatment to obtain CZTS thin film, (c) deposited CdS buffer layer via CBD, (d) post-annealing of the CZTS/CdS heterojunction, (e) deposited ITO layer by magnetron sputtering, (f) final structural representation of the CZTS thin film solar cell.

Characterization methods

The structural and phase properties of CZTS films were detected by X-ray diffraction (XRD) diffractometer (Rigaku Ultima IV) operating with 2θ range from 10° to 80° and Raman measurement (LABRAM-HR) with excitation at 532 nm. Surface and cross-section images morphology of CZTS films and devices were detected by SEM (SUPRA 55) under 3 kV. EDS (BRUKER QUANTAX 200) at 15 kV was used to characterize chemical composition. Current density-voltage (J–V) characterization was performed on Keithley 2400 Source Meter by using a solar simulator (Zolix SS150A) with an AM1.5 G illumination (100 mW/cm^2, 25 °C) calibrating with a standard Si reference cell. The external quantum efficiency (EQE) spectra were detected by a Zolix solar cell QE/IPCE measurement system (SCS 100) and a Keithley 2400 source meter. Capacitance-voltage (C-V) measurements (Keithley 4200) were carried out using an impedance analyzer at a frequency of 50 kHz with a DC bias voltage sweeping from -1.0 to 0 V, and conducted at an AC amplitude of 30 mV and frequency of 50 kHz under the dark at room temperature. DLCP measurement was performed with frequency of 1 kHz at a DC bias from −0.25 to 0 V and AC amplitude from 0.015 to 0.14 V. The electrochemical impedance spectroscopy (EIS) was conducted on CHI600E Electrochemical Workstation at 0 bias potential in darkness. Time-resolved photoluminescence (TR-PL) characterization was performed on the devices using time-correlated single photon counting (TCSPC) (FluoTime 300, PicoQuant Gmbh), with power of 50 mW and an excitation wavelength of 532 nm.

Results and discussion

Characterization of CZTS thin films

XRD was used to investigate the effect of sulfurization temperature on the structural properties of the CZTS thin films deposited on Mo-coated glass substrates. A comparison of XRD patterns of the as-deposited and sulfurized CZTS thin films at different temperatures (590 °C, 600 °C, and 610 °C) is presented in Figure 2a. Upon sulfurization, non-characteristic peaks disappeared, and the characteristic peak intensities exhibited obvious improvement, indicating enhanced crystallinity. The peaks

labeled as (1 0 1), (1 1 2), (2 0 0), (2 2 0), (3 1 2), (0 0 8), and (3 3 2) were attributed to kesterite CZTS or zincblende phases (ZnS) and/or Cu_2SnS_3. The diffraction peak at 40° was assigned to the Mo substrate underneath. From 590 °C to 610 °C, a gradual transition could be clearly seen from the shift of the diffraction peaks to smaller angles, indicating improved crystallinity and larger grains size (Figure 2a).

Owing to the same crystal structure of ZnS and Cu_2SnS_3, the crystal structure and phase purity of the CZTS film could not be distinguished by XRD. Therefore, the films were further investigated by Raman spectroscopy. The Raman spectra of the CZTS films sulfurized at different temperatures are shown in Figure 2b. No obvious shift of vibration could be observed for the different sulfurization temperature samples, confirming the absence of any impurity phases. All the labeled vibrations in the Raman spectra were the characteristic modes of kesterite CZTS. However, the strong peak at 287 and 337 cm^{-1} have been reported in the literature to be the main vibration modes of kesterite CZTS.[24] Besides, the films sulfurized at 590 °C, 600 °C and 610 °C showed one peak near 360 cm^{-1}, which could be assigned to the characteristic peaks of $CuSnS_3$. [25, 26] The film sulfurization at 610 °C showed improved crystallinity and suppressed secondary phases. Moreover, the main peaks (287 and 337 cm^{-1}) of CZTS films revealed a minor shift to the higher wavelength with the increase in sulfurization temperature. Several factors that may contribute to this phenomenon, mainly phonon confinement, strain, non-stoichiometry in films, and defects in the crystal lattice.[27, 28] The peak seems to be more broad and sharpen at 287 cm^{-1}, which may be attributed to the Cu/Zn disorder caused by the cooling rate after annealing.[29] From the perspective of XRD analysis and Raman spectroscopy, a high-quality CZTS absorber film with excellent crystallinity and undetectable impurity phase was obtained at 600 °C sulfurization temperature. For low temperature, some unavoidable phases, except for some secondary and ternary phases (ZnS, Cu_2SnS_3, and Cu_3SnS_4), were witnessed.

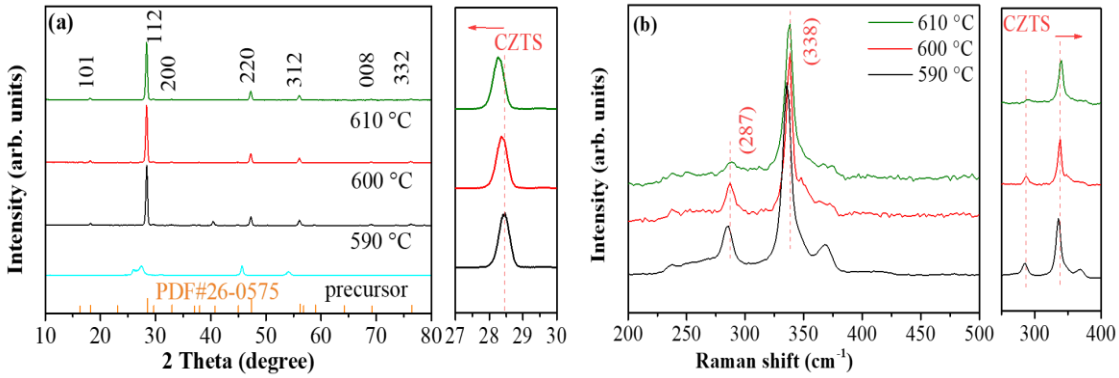

Figure 2. (a) The X-ray diffraction (XRD) patterns and (b) Raman spectra of the CZTS thin films with different post-sulfurization temperatures. The enlargement of the (112) diffraction peak of the films is shown in (a) right, enlargement of the Raman shift at 287 cm^{-1} and 337 cm^{-1} is shown in (b) right.

SEM analysis was conducted for the films prepared at different sulfurization temperatures were accomplished to further investigate the effect of different annealing temperatures on the grain and film quality. Figures 3(a)-(c) show the surface morphology of the thin films sulfurized at 590 °C – 610 °C, and a gradual increase in the grain size and compactness was observed. The films were composed of large grains (few micrometers); however, a few voids could be clearly seen on the surface of CZTS (Figure 3c). Compared with the absorber film obtained at 610 °C, the grain size at 590 °C was smaller and non-uniform. The prepared CZTS absorber layer in this work showed lower porosity and larger uniform grains compared with the oxide route.[23] All the three types of prepared films showed uniform morphology and large extended grains from top to bottom, as depicted in Figures 3 (d) - (e). The segregation of smaller grains, voids, and secondary phases was not observed at the interfaces. As all XRD and Raman peaks were attributed to CZTS, the content of any other phase was below the detection limit of these measurement techniques. In contrast to the state-of-the-art devices' fabrication techniques, all the films prepared via PLD method showed optimistic crystallinity and back contact. This phenomenon may be a consequence of the compactness of the amorphous structure of the precursors fabricated by PLD. The thickness of the absorption layer reached 1.4 µm, thicker than the CZTS device

prepared with PLD in other reports. [30, 31] Many studies have been reported that a noticeable affection for the open-circuit voltage and the fill factor caused by thickness. The morphology of the thick absorption film grown under similar conditions was also suggested to be better than that of the thin absorption film. Thin films are usually accompanied by reduced grain size and increased density of shunt paths; the latter was demonstrated by the fact that the shunt resistance of the device decreased with decreasing thickness. [32, 33] The thin MoS_2 layer could be attributed to the two-zone furnace and the shorter holding time, which could effectively control the temperature, heating time, and diffusion of sulfur at the same time. The sulfur vapors provided by sulfur powder could remain in the annealing atmosphere for a longer time than gaseous sulfur source.

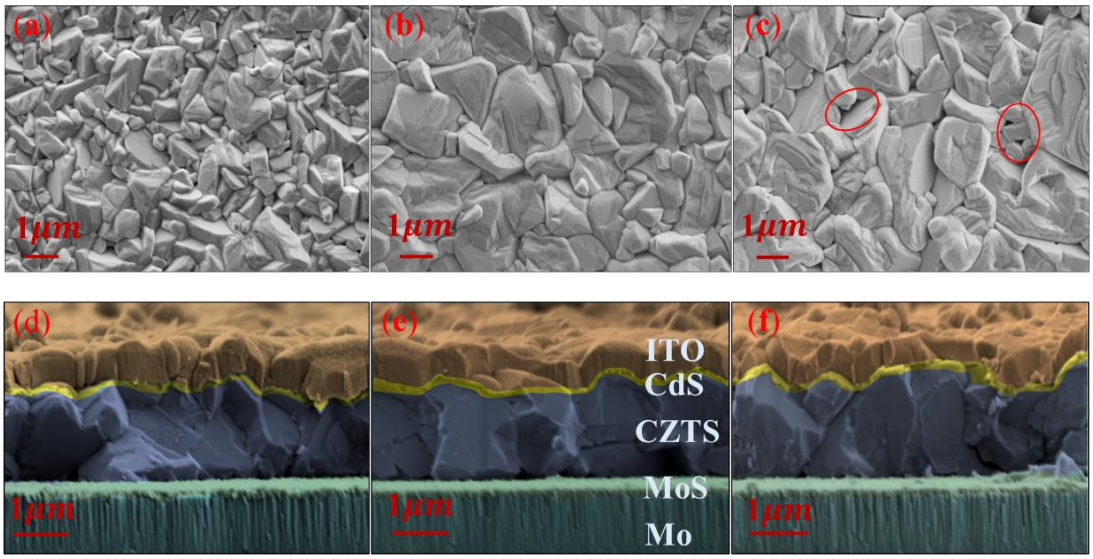

Figure 3. SEM top-view images of the CZTS thin-films with different post-sulfurization heat treatment temperatures, (a) 590 °C, (b) 600 °C, (c) 610 °C, respectively. SEM cross section images of the CZTS thin-films with different post-sulfurization heat treatment temperatures, (d) 590 °C, (e) 600 °C, and (f) 610 °C. The length of red scale bar at the left bottom of each image represents 1μm.

SEM analysis, demonstrated the CZTS films prepared at 600 °C showed much better morphology and compactness. Thus, the film preparation process depending on the precursor prepared under different laser energies (50, 150, 250 mJ) and substrate

temperatures (100 °C to 400 °C). SEM images of the precursor films obtained at different laser energies are shown in Figures S3 (a)–(c). They exhibiting no obvious crystallization. The small droplets on the film were metal balls containing three components of Cu-Zn-Sn due to the ablation process of the target material.[34] They could be removed by KCN etching; however, pinholes and voids may be left in the precursor, and this situation is undesirable for manufacturing solar cells.[30] In the present work, removing these droplets did not seem necessary because after the annealing process, copper atoms diffused effectively in the film. In addition, Raman spectroscopy did not detect Cu-containing secondary phase in the annealed film. However, the film obtained under the condition of high laser energy can obviously have increased large particles, and more large holes appeared in the film after the precursor films were sulfurized [Figures S3 (d)–(f), Supporting information]. The reason for these problems may be that the high laser energy beam could sinter and sputter more large particles from the target. Though the film prepared under the condition of low laser energy was more uniform, the as-deposited film fell off after high-temperature annealing. This phenomenon may be explained by the low plume energy and the low adhesion of the precursor film on the substrate. Likewise, the preparation of CZTS thin film was found to be critically dependent on substrate temperature. As shown in Figures S4 (a)-(h), Supporting Information, the precursor films were almost independent of substrate temperature. However, upon sulfurization, the crystal grains and the pores in the film increased. These phenomena could be attributed to thermal stress during preparation. The XRD patterns of all the samples indicated kesterite CZTS phase (Figure S5, Supporting information). Thus, for the preparation of solar cell, a moderate laser energy of 150 mJ and a substrate temperature of 200 °C was utilized.

The composition of target and absorber film detected by EDS is shown in Table 1. Comparison of the elemental composition of the target material with that of the precursor, showed that the element of the target material was transferred to the substrate smoothly. To confirm the composition uniformity of 4×4 cm^2 precursor film, different regions of precursor film were analyzed by EDS in Figure S6 and table S1 which showed that the locations of the Cu, Zn, Sn and S elements were nearly uniform across

the entire plane. The relatively high copper content may be attributed to the high-energy laser we chosen in this work. The composition changes in of the precursor may be the direct consequence of non-directional evaporation of the volatile components of ZnS and SnS from the target. In the post-sulfurized sample, the relatively higher Cu content could be assigned to the evaporation and diffusion of the secondary phase with the increase in annealing temperature.

Table 1. The component ratio of CZTS for targets, precursor thin films and film with different post-sulfurization temperatures.

	Cu(at%)	Zn(at%)	Sn(at%)	S(at%)	Cu/(Zn+Sn)	Zn/Sn	S/(Cu+Zn+Sn)
Target	24.77	15.64	11.24	48.35	0.92	1.39	0.93
Precursor	24.38	12.83	12.79	50.90	0.95	1.00	1.04
590 °C	24.06	10.33	10.54	55.07	1.15	0.98	1.18
600 °C	24.17	11.13	11.18	53.51	1.08	0.99	1.12
610 °C	24.66	11.42	12.28	51.64	1.04	0.93	1.03

Device characterization

Figure 4(a)–(d) shows the statistical distribution of the three devices' performance parameters, including V_{OC}, short circuit current (J_{SC}), fill factor (FF) and PCE. Sixteen devices were prepared on each category of absorption layer films, and acceptable performance changes between the individual devices further demonstrated the good uniformity of the film and the reproducibility of the device fabrication process. The effect of post-sulfurization temperature on the device parameters reflected the necessity and importance of proper annealing temperature for photovoltaic performance. Combined with XRD, Raman and SEM analysis, the results showed that the performance of the solar cell was closely related to the absorber film crystallinity, large crystal grains, and standard stoichiometric ratio, which may all effectively reduce the interface defect concentration of the device and restrain the compound loss.

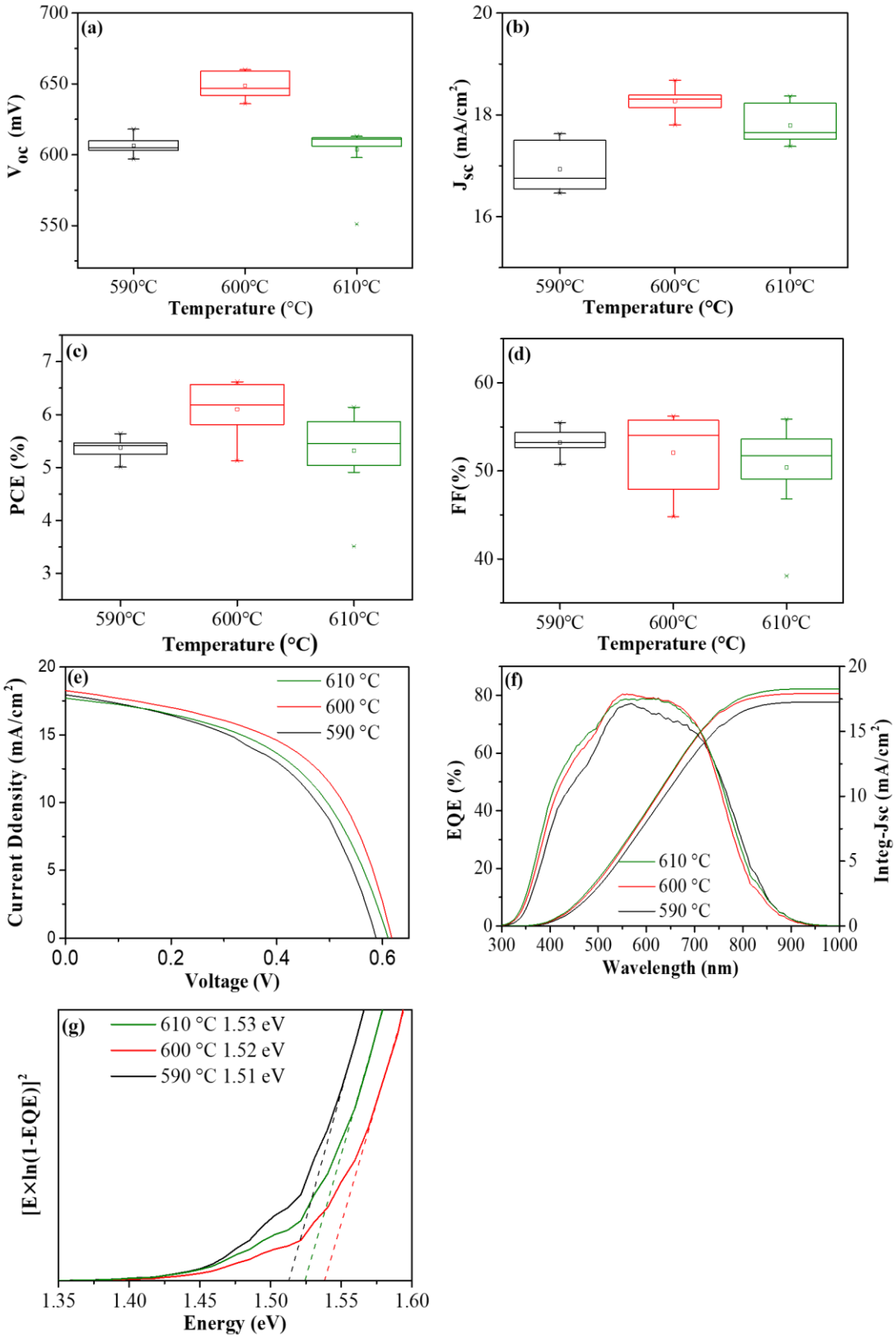

Figure 4. (a)-(d) Statistical box plot of devices performance parameters for 16 solar cells obtained from each variety of absorber film fabricated at different temperatures, (a) open-circuit voltage (V_{OC}), (b) short-circuit current density (J_{SC}), (c) power

conversion efficiency (PCE), (d) fill factor (FF). (e) *J-V* curves of best devices fabricated from the CZTS absorber films sulfurized at 590 °C -610 °C. (f) EQE spectra and corresponding integrated J_{SC} for the devices with CZTS obtain with sulfurization temperature at 590 °C -610 °C. (g) Bandgap calculated from the EQE.

The *J-V* curves and EQE spectra of the CZTS solar cells sulfurized at different temperatures are shown in Figures 4(e) and (f), respectively. The corresponding device parameters, including V_{OC}, J_{SC}, FF, and PCE are summarized in Table 2. To date, the most efficient solar cells prepared by PLD could demonstrate PCE = 5.4%, V_{OC} = 673 mV, FF = 53.0%, and J_{SC} = 15.2 mA,[23] whereas the champion device in the present study exhibited a higher efficiency of 6.62%, with a J_{SC} of 18.4 mA/cm^2, a V_{OC} of 642 mV, and FF of 56.21%. Regardless of the annealing temperature, this device obtained a J_{SC} of more than 17 mA/cm^2 and most of the devices obtained a higher *FF* which is attributed to the excellent film quality. The EQE characterization for four devices in Figure 4(c), the spectral response of the device sulfurized at 600 °C was much encouraging in the range of 500–900 nm. Importantly, all the devices had a high quantum response with EQE values near 80%, indicating lesser recombination losses at high-quality CZTS/CdS interface and the suppressed detrimental defects in the absorber layer.[35] The integrated J_{SC} value calculated using the computational formula ($J_{SC} = \int_{\lambda_1}^{\lambda_2} F(\lambda)EQE(\lambda)d\lambda$) for the three devices were 17.2, 17.9, and 18.2 mA/cm^2 respectively, where $F(\lambda)$ is the photon flux (cm $^{-2}$ nm $^{-1}$ s $^{-1}$). Compared with the result measured under AM 1.5G and 1-sun illumination (Table 2), the integrated J_{SC} was in close agreement with the obtained *J-V* measurement results. The bandgaps (Figure 4d) of the absorbers were determined by the [E × ln(1-EQE)]^2 from EQE curves were 1.51, 1.52, and 1.53 eV for different temperature, which was close to the optimal band gap energy required for thin film solar cell.

Table 2. Device performance of CZTS solar cells with different sulfurization temperature.

Temperature	η (%)	V_{OC} (mV)	J_{SC} (mA/cm^2)	FF (%)
590 °C	5.64	597	17.50	55.49
600 °C	6.62	642	18.40	56.21
610 °C	6.14	612	18.27	55.87

The heterojunction-dependent built-in voltage (V_{bi}) of the three types of devices were measured through *C-V* analysis to scrutinize the effect of sulfurization temperature on charge densities distribution, as shown in Figure 5(a). Through the theoretical calculation formula[36] of V_{bi} : $\frac{1}{C^2} = \frac{2(V_{bi}-V)}{eA^2\varepsilon_0\varepsilon_S N^*}, V_{bi} = \frac{eA^2\varepsilon_0\varepsilon_S N^*}{2C^2} + V$, the value of V_{bi} could be identified by linear fitting and x-intercept of the tangent line of curves.[37] Usually, the linear region near the bias voltage of 0 V is used for linear fitting.[38] The V_{bi} of the device (1005 mV) sulfurized at 600 °C was larger than that of the other devices (910 mV, and 980 mV), indicating a superior CZTS/CdS heterojunction interface. The influence of free carriers and bulk defects in the absorber layer is generally reflected by *DLCP*, while that of interface trap states is usually explained by *C-V*. Thus, *C-V* analysis and *DLCP* measurement were also carried out (Figure 5b). The concentration difference between *C-V* and *DLCP*($N_{c\text{-}v}$-N_{DLCP}) at zero bias could reflect the trap state at the CZTS/CdS interface. [5, 16, 39] The following equations [40] expressed the plots of $N_{c\text{-}v}$ and N_{DLCP} for the profiling depth *x*:

$$\begin{cases} N_{c-v} = \dfrac{C^3}{qA^2\varepsilon_0\varepsilon_S}\left(\dfrac{dC}{dV}\right)^{-1}, \\ N_{DLCP} = -\dfrac{C_0^3}{2q\varepsilon_0\varepsilon_S A^2 C_1}, \\ x = \varepsilon_0\varepsilon_s A/C \end{cases}$$

where A is the device active area, ε_0 and ε_s are the vacuum dielectric constant ($\approx$ 8.854 × 10^{-12} Fm^{-1}) [41] and the relative dielectric constant of CZTS ($\approx$7.1) [42]; C is the measure capacitance (5.2×10^{-9}-1×10^{-8} F); C_0 is the minimum limiting value of capacitance as AC amplitude approaches 0.[43] The interface trap density ($N_{C\text{-}V}$-N_{DLCP} at

0 bias) for different devices were 1.8×10^{16}, 9.0×10^{17}, and 1.2×10^{16} cm^{-3}. The charge density of the *C-V* and *DLCP* of the device prepared at 600 °C sulfurization was significantly lower than that of other devices, demonstrating superior film quality, suppressed detrimental defects of the CZTS. The device interface has the highest defect density at 610 °C. This may be due to abnormal grain growth caused by high-temperature annealing, or the production of craters, which seriously affects the quality of the film. The *N-DLCPs* of the three devices were 8.1×10^{16}, 3.1×10^{16}, and 5.5×10^{16} cm^{-3}, respectively. Even though the carrier concentration does not change much, the defect concentration displayed by the CZTS film at 600 °C was much lower. This finding could also be explained by the SEM analysis of the CZTS film surface. Compared with other films, the film sulfurized at 600 °C was smoother, and denser than the other films, and it was composed of large and tight bonded grains. Thus, the interface was reorganized and the deep energy level defect was considerably suppressed. In addition, it had the largest depletion width of X_d = 167 nm (V = 0 V). When defining the ratio of *w/d* (*w* refers to the width of the depletion zone at 0 bias, and d represents the thickness of the absorber layer), the diffusion length of low-rate solar cells (such as crystalline silicon and dye-sensitized solar cells) is usually larger.[44] Those thin-film solar cells with low-mobility life, such as CIGS and CdTe solar cells, have a larger *w/d*.[44] The *w/d* value of the champion CZTS solar cell prepared by the PLD in the present study is comparable to the *w/d* value of the high-efficiency (11.1%) CZTS solar cell prepared by the sputtering method.[6] This finding may be a key factor to obtain such high short-circuit current density.

EIS has been widely applied in photovoltaic to demonstrate charger transport and recombination in CZTS solar cells.[45] In the present study, the characteristics of minority carrier recombination was determined by EIS measurement conducted at 0V bias (Figure 5c). The intercept of the x-axis and the diameter of the semicircle corresponded to series resistance (R_S) and recombination resistance (R_{rec}) respectively.[41] The relevant parameters of different sulfurization temperature devices obtained by fitting are shown in Table 3. The device obtained at 600 °C sulfurization temperature showed the minimum series and maximum recombination resistance,

signifying a favorability for charge transport mechanism benefitting from the superiors thin-film and interface quality.[46] Therefore, the efficient separation and transportation of charge carriers led to obtain excellent photoelectric properties. The time-resolved photoluminescence (*PL*) of the champion device was also studied, and the result is presented in Figure 5d. Bi-exponential decay function was used to fit the *PL* intensity decay,[47] and calculate carrier lifetime by using the formula: $\tau_{avg} = \frac{A_1 t_1^2 + A_2 t_2^2}{A_1 t_1 + A_2 t_2}$. The obtained average *PL* lifetime was 1.2 ns, which was comparable to the value obtained by solution preparation with the similar efficiency.[15] However, this value was relatively low compared with that of state-of-the-art solar cells leading to a reasonable efficiency of 6.62%.

Table 3. Summary of results derived from C-V and DLCP measurements and EIS

Device	N_{CV} (cm^{-3})	N_{DLCP} (cm^{-3})	Interface state response (relative values)	Depletion width (nm)	R_S (Ω)	R_{rec} (Ω)
590 °C	9.9×10^{16}	8.1×10^{16}	1.8×10^{16}	113	71.6	47454
600 °C	4.0×10^{16}	3.1×10^{16}	9.0×10^{17}	167	26.4	130570
610 °C	6.7×10^{16}	5.5×10^{16}	1.2×10^{16}	140	40.1	70294

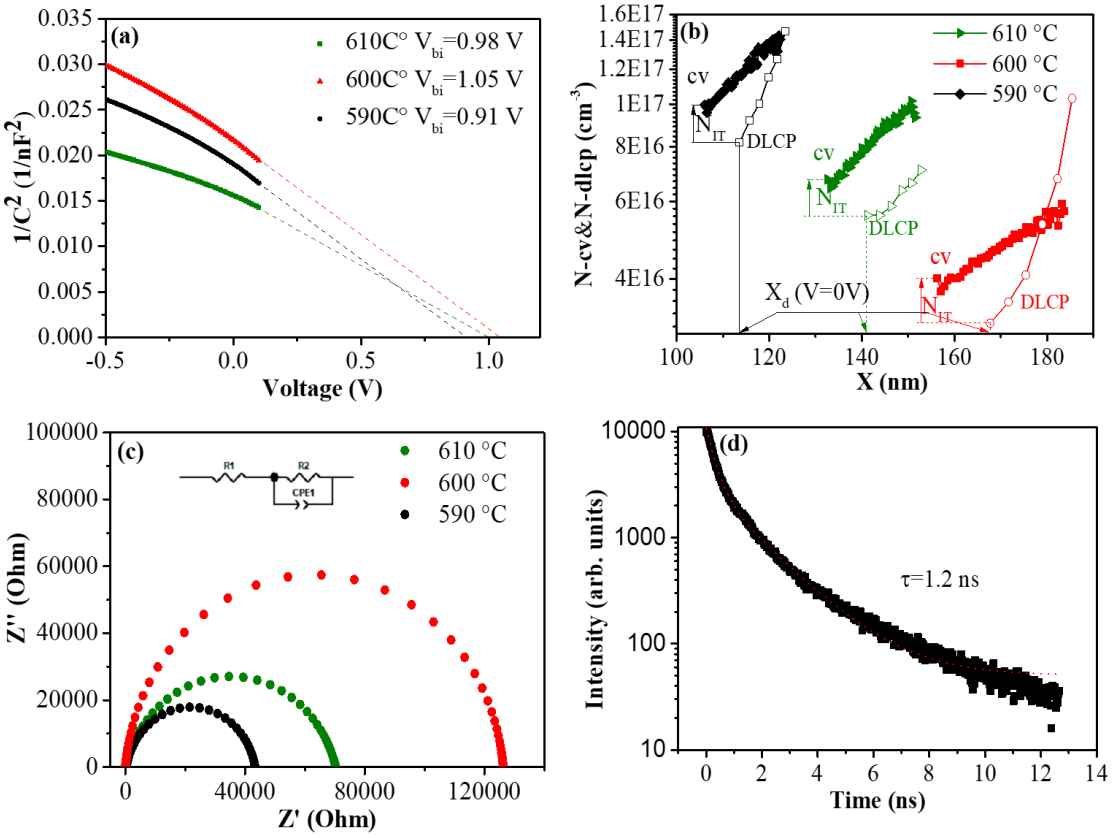

Figure 5. (a) $1/C^2 - V$ plots, (b) CV and *DLCP* profiles, (c) EIS Nyquist plots of the devices with different annealing temperatures under a 0v bias, (d) $TR - PL$ curves of CZTS solar cells.

Conclusions

In this work, CZTS thin films were obtained by PLD from a quaternary target and post-sulphuration process. The as-deposited CZTS precursors could be transformed and crystallized into high-quality CZTS absorbers with the following characteristics: kesterite structure, no obvious secondary or ternary phases, high (112) orientation, and dense polycrystalline grains with controlled composition on the optimized substrate temperature of 200 °C, laser pulse energy of 150 mJ and sulfurization temperature of 600 °C. Substrate-structured CZTS thin-film solar cells with Mo/CZTS/CdS/ITO/Ag were fabricated with a remarkable boost (from 597 to 642 mV) in the V_{OC} and J_{SC} (from 17.50 mA/cm^2 to 18.40 mA/cm^2), leading to an encouraging PCE of 6.62 % without anti-reflective coating MgF_2. It was the highest reported efficiency for a PLD-processed

CZTS thin film solar cell. This significantly improved efficiency was closely related to lower series resistance, reduced grain boundary effects, superior interface quality, and a suitable depletion width of 167 nm. Thus, the pulsed laser deposited and sulfurized process demonstrated a remarkable potential for highly efficient CZTS solar cells.

Acknowledgements

This work was supported by National Natural Science Foundation of China (No. 62074102), Science and Technology plan project of Shenzhen (20200826143347001, JCYJ20190808153409238) China, Key Project of Department of Education of Guangdong Province (No. 2018KZDXM059) China.

References

[1] G.M. Wilson, M. Al-Jassim, W.K. Metzger, S.W. Glunz, P. Verlinden, G. Xiong, L.M. Mansfield, B.J. Stanbery, K. Zhu, Y. Yan, J.J. Berry, A.J. Ptak, F. Dimroth, B.M. Kayes, A.C. Tamboli, R. Peibst, K. Catchpole, M.O. Reese, C.S. Klinga, P. Denholm, M. Morjaria, M.G. Deceglie, J.M. Freeman, M.A. Mikofski, D.C. Jordan, G. TamizhMani, D.B. Sulas-Kern, The 2020 photovoltaic technologies roadmap, J. Phys. D-Appl. Phys. 53 (2020). https://doi.org/1361-6463/ab9c6a.

[2] M.A. Green, K. Emery, Y. Hishikawa, W. Warta, E.D. Dunlop, D.H. Levi, A.W.Y. Ho-Baillie, Solar cell efficiency tables (version 49), Prog. Photovoltaics: Research and Applications. 25 (2017) 3-13. https://doi.org/10.1002/pip.2855.

[3] S.-Y. Li, C. Hägglund, Y. Ren, J.J.S. Scragg, J.K. Larsen, C. Frisk, K. Rudisch, S. Englund, C. Platzer-Björkman, Optical properties of reactively sputtered Cu_2ZnSnS_4 solar absorbers determined by spectroscopic ellipsometry and spectrophotometry, Sol. Energy Mater. Sol. Cells. 149 (2016) 170-178. https://doi.org/10.1016/j.solmat.2016.01.014.

[4] P.K. Sarswat, M.L. Free, A study of energy band gap versus temperature for Cu_2ZnSnS_4 thin films, Physica B. 407 (2012) 108-111. https://doi.org/10.1016/j.physb.2011.09.134.

[5] W. Wang, M.T. Winkler, O. Gunawan, T. Gokmen, T.K. Todorov, Y. Zhu, D.B. Mitzi, Device Characteristics of CZTSSe Thin-Film Solar Cells with 12.6% Efficiency, Adv. Energy Mater. 4 (2014). https://doi.org/10.1002/aenm.201301465.

[6] C. Yan, J. Huang, K. Sun, S. Johnston, Y. Zhang, H. Sun, A. Pu, M. He, F. Liu, K. Eder, L. Yang, J.M. Cairney, N.J. Ekins-Daukes, Z. Hameiri, J.A. Stride, S. Chen, M.A. Green, X. Hao, Cu_2ZnSnS_4 solar cells with over 10% power conversion efficiency enabled by heterojunction heat treatment, Nat. Energy. 3 (2018) 764-772. https://doi.org/10.1038/s41560-018-0206-0.

[7] W. Shockley, H.J. Queisser, Detailed Balance Limit of Efficiency of p-n Junction Solar Cells, J. Appl. Phys. 32 (1961) 510-519. https://doi.org/10.1063/1.1736034.

[8] T.G. Sanchez, X. Mathew, N.R. Mathews, Obtaining phase-pure CZTS thin films by annealing vacuum evaporated CuS/SnS/ZnS stack, J. Cryst. Growth. 445 (2016) 15-23. https://doi.org/10.1016/j.jcrysgro.2016.03.039.

[9] B. Shin, O. Gunawan, Y. Zhu, N.A. Bojarczuk, S.J. Chey, S. Guha, Thin film solar cell with 8.4% power conversion efficiency using an earth-abundant Cu_2ZnSnS_4 absorber, Prog. Photovoltaics: Research and Applications. 21 (2013) 72-76. https://doi.org/10.1002/pip.1174.
[10] S. Das, R.N. Bhattacharya, K.C. Mandal, Performance limiting factors of $Cu_2ZnSn(S_xSe_{1-x})_4$ solar cells prepared by thermal evaporation, Sol. Energy Mater. Sol. Cells. 144 (2016) 347-351. https://doi.org/10.1016/j.solmat.2015.09.012.
[11] H. Yoo, J. Kim, Growth of Cu_2ZnSnS_4 thin films using sulfurization of stacked metallic films, Thin Solid Films. 518 (2010) 6567-6572. https://doi.org/10.1016/j.tsf.2010.03.058.
[12] X. Liu, Y. Huang, J. Yun, X. Wen, Z. Lu, T. Zhang, H. Cui, W. Li, C.-Y. Lee, S. Xu, X. Hao, G. Conibeer, Characterization of a Cu_2ZnSnS_4 solar cell fabricated by sulfurization of metallic precursor Mo/Zn/Cu/Sn, Phys. Status Solidi (a). 212 (2015) 2074-2079. https://doi.org/10.1002/pssa.201431942.
[13] P. Bras, J. Sterner, C. Platzer-Björkman, Investigation of blister formation in sputtered Cu_2ZnSnS_4 absorbers for thin film solar cells, J. Vac. Sci. Technol. A: Vacuum, Surfaces, and Films. 33 (2015). https://doi.org/10.1116/1.4926754.
[14] D.K. Kaushik, T.N. Rao, A. Subrahmanyam, Studies on the disorder in DC magnetron sputtered Cu_2ZnSnS_4(CZTS) thin films grown in sulfide plasma, Surf. Coat. Technol. 314 (2017) 85-91. https://doi.org/10.1016/j.surfcoat.2016.09.034.
[15] Z. Su, G. Liang, P. Fan, J. Luo, Z. Zheng, Z. Xie, W. Wang, S. Chen, J. Hu, Y. Wei, C. Yan, J. Huang, X. Hao, F. Liu, Device Postannealing Enabling over 12% Efficient Solution-Processed Cu_2ZnSnS_4 Solar Cells with Cd^{2+} Substitution, Adv. Mater. 32 (2020) e2000121. https://doi.org/10.1002/adma.202000121.
[16] T. Todorov, H.W. Hillhouse, S. Aazou, Z. Sekkat, O. Vigil-Galán, S.D. Deshmukh, R. Agrawal, S. Bourdais, M. Valdés, P. Arnou, D.B. Mitzi, P.J. Dale, Solution-based synthesis of kesterite thin film semiconductors, J. Energy. Phys. 2 (2020). https://doi.org/10.1088/2515-7655/ab3a81.
[17] P. Fan, Z. Xie, G. Liang, M. Ishaq, S. Chen, Z. Zheng, C. Yan, J. Huang, X. Hao, Y. Zhang, Z. Su, High-efficiency ultra-thin Cu_2ZnSnS_4 solar cells by double-pressure sputtering with spark plasma sintered quaternary target, J. Energy Chem. 61 (2021) 186-194. https://doi.org/10.1016/j.jechem.2021.01.026.
[18] P. Willmott, Deposition of complex multielemental thin films, Prog. Surf. Sci. 76 (2004) 163-217. https://doi.org/10.1016/j.progsurf.2004.06.001.
[19] D.R. NORTON, Pulsed Laser Deposition of Complex Materials: Progress, Pulsed laser deposition of thin films: applications-led growth of functional materials. (2007) 1. https://doi.org/10.1002/0470052120.
[20] K. Moriya, K. Tanaka, H. Uchiki, Fabrication of Cu_2ZnSnS_4 Thin-Film Solar Cell Prepared by Pulsed Laser Deposition, Jpn. J. Appl. Phys. 46 (2007) 5780-5781. https://doi.org/10.1143/jjap.46.5780.
[21] K. Moriya, K. Tanaka, H. Uchiki, Cu_2ZnSnS_4 Thin Films Annealed in H_2S Atmosphere for Solar Cell Absorber Prepared by Pulsed Laser Deposition, Jpn. J. Appl. Phys. 47 (2008) 602-604. https://doi.org/10.1143/jjap.47.602.
[22] X. Jin, C.C. Yuan, G.S. Jiang, W.F. Liu, C.F. Zhu, Pulsed laser deposition of Cu_2ZnSnS_4 thin films from single quaternary sulfide target prepared by combustion method, Mater. Lett. 175 (2016) 180-183. https://doi.org/10.1016/j.matlet.2016.04.046.
[23] M. Gansukh, S. López Mariño, M. Espindola Rodriguez, S.L.J. Engberg, F.M.A. Martinho, A. Hajijafarassar, N.C. Schjødt, E. Stamate, O. Hansen, J. Schou, S. Canulescu, Oxide route for production of Cu_2ZnSnS_4 solar cells by pulsed laser deposition, Sol. Energy Mater. Sol. Cells. 215 (2020). https://doi.org/10.1016/j.solmat.2020.110605.

[24] M. Dimitrievska, A. Fairbrother, X. Fontané, T. Jawhari, V. Izquierdo-Roca, E. Saucedo, A. Pérez-Rodríguez, Multiwavelength excitation Raman scattering study of polycrystalline kesterite Cu_2ZnSnS_4 thin films, Appl. Phys. Lett. 104 (2014). https://doi.org/10.1063/1.4861593.
[25] P.A. Fernandes, P.M.P. Salomé, A.F. da Cunha, Study of polycrystalline Cu_2ZnSnS_4 films by Raman scattering, J. Alloy. Compd. 509 (2011) 7600-7606. https://doi.org/10.1016/j.jallcom.2011.04.097.
[26] P.A. Fernandes, P.M.P. Salomé, A.F. da Cunha, Cu_xSnS_{x+1}(x = 2, 3) thin films grown by sulfurization of metallic precursors deposited by dc magnetron sputtering, Phys. Status Solidi (c). (2010) NA-NA. https://doi.org/10.1002/pssc.200982746.
[27] J. Ge, Y. Wu, C. Zhang, S. Zuo, J. Jiang, J. Ma, P. Yang, J. Chu, Comparative study of the influence of two distinct sulfurization ramping rates on the properties of Cu_2ZnSnS_4 thin films, Appl. Surf. Sci. 258 (2012) 7250-7254. https://doi.org/10.1016/j.apsusc.2012.02.141.
[28] S. Kermadi, S. Sali, F. Ait Ameur, L. Zougar, M. Boumaour, A. Toumiat, N.N. Melnik, D.W. Hewak, A. Duta, Effect of copper content and sulfurization process on optical, structural and electrical properties of ultrasonic spray pyrolysed Cu_2ZnSnS_4 thin films, Mater. Chem. Phys. 169 (2016) 96-104. https://doi.org/10.1016/j.matchemphys.2015.11.035.
[29] J.J.S. Scragg, L. Choubrac, A. Lafond, T. Ericson, C. Platzer-Björkman, A low-temperature order-disorder transition in Cu_2ZnSnS_4 thin films, Appl. Phys. Lett. 104 (2014). https://doi.org/10.1063/1.4863685.
[30] A. Cazzaniga, A. Crovetto, C. Yan, K.W. Sun, X.J. Hao, J.R. Estelrich, S. Canulescu, E. Stamate, N. Pryds, O. Hansen, J. Schou, Ultra-thin Cu_2ZnSnS_4 solar cell by pulsed laser deposition, Sol. Energy Mater. Sol. Cells. 166 (2017) 91-99. https://doi.org/10.1016/j.solmat.2017.03.002.
[31] M. Heidariramsheh, M. Haghighi, M.M. Dabbagh, S.M. Mahdavi, Pure sulfide Cu_2ZnSnS_4 layers through a one-step low-temperature PLD technique: Insight into simulation on modified back contact to overcome the barrier of MoS_2, Mater. Sci. Eng. B-Adv. Funct. Solid-State Mater. 262 (2020). https://doi.org/10.1016/j.mseb.2020.114701.
[32] Y. Ren, J.J.S. Scragg, C. Frisk, J.K. Larsen, S.-Y. Li, C. Platzer-Björkman, Influence of the Cu_2ZnSnS_4 absorber thickness on thin film solar cells, Phys. Status Solidi(a). 212 (2015) 2889-2896. https://doi.org/10.1002/pssa.201532311.
[33] O. Lundberg, M. Bodegård, J. Malmström, L. Stolt, Influence of the Cu(In,Ga)Se_2 thickness and Ga grading on solar cell performance, Prog. Photovoltaics. 11 (2003) 77-88. https://doi.org/10.1002/pip.462.
[34] S. Kala, H. Kaur, A. Rastogi, V.N. Singh, T.D. Senguttuvan, Structural and opto-electronic features of pulsed laser ablation grown Cu2ZnSnS4 films for photovoltaic applications, J Alloy Compd, 658 (2016) 324-330.
[35] G.-X. Liang, Y.-D. Luo, S. Chen, R. Tang, Z.-H. Zheng, X.-J. Li, X.-S. Liu, Y.-K. Liu, Y.-F. Li, X.-Y. Chen, Z.-H. Su, X.-H. Zhang, H.-L. Ma, P. Fan, Sputtered and selenized Sb_2Se_3 thin-film solar cells with open-circuit voltage exceeding 500 mV, Nano Energy. 73 (2020). https://doi.org/10.1016/j.nanoen.2020.104806.
[36] S.M. Sze, Physics of Semiconductor Devices 3rd Edition, New York, New York: John Wiley & Sons, 2007, pp. 77-133. https://doi.org/10.1002/9780470068328.ch2
[37] M. Ishaq, H. Deng, U. Farooq, H. Zhang, X. Yang, U.A. Shah, H. Song, Efficient Copper-Doped Antimony Sulfide Thin-Film Solar Cells via Coevaporation Method, Sol. Rrl. 3 (2019). https://doi.org/10.1002/solr.201900305.
[38] J. Moore, C. J. Hages, N. Carter, R. Agrawal and M. Lundstrom, "The physics of Vbi-related IV crossover in thin film solar cells: Applications to ink deposited CZTSSe," 2013 IEEE 39th Photovoltaic

Specialists Conference (PVSC), 2013, pp. 3255-3259. https://doi.org/10.1109/PVSC.2013.6745146.
[39] J. Li, Y. Huang, J. Huang, G. Liang, Y. Zhang, G. Rey, F. Guo, Z. Su, H. Zhu, L. Cai, K. Sun, Y. Sun, F. Liu, S. Chen, X. Hao, Y. Mai, M.A. Green, Defect Control for 12.5% Efficiency $Cu_2ZnSnSe_4$ Kesterite Thin-Film Solar Cells by Engineering of Local Chemical Environment, Adv. Mater. 32 (2020) e2005268. https://doi.org/10.1002/adma.202005268.
[40] T. Kirchartz, K. Ding, U. Rau, Fundamental Electrical Characterization of Thin-Film Solar Cells, in: Advanced Characterization Techniques for Thin Film Solar Cells, pp. 33-60. https://doi.org/10.1002/9783527699025.ch2.
[41] Y. Du, S. Wang, Q. Tian, Y. Zhao, X. Chang, H. Xiao, Y. Deng, S. Chen, S. Wu, S. Liu, Defect Engineering in Earth-Abundant $Cu_2ZnSn(S,Se)_4$ Photovoltaic Materials via Ga^{3+}-Doping for over 12% Efficient Solar Cells, Adv. Funct. Mater. 31 (2021). https://doi.org/10.1002/adfm.202010325.
[42] O. Gunawan, T. Gokmen, C.W. Warren, J.D. Cohen, T.K. Todorov, D.A.R. Barkhouse, S. Bag, J. Tang, B. Shin, D.B. Mitzi, Electronic properties of the Cu2ZnSn(Se,S)4 absorber layer in solar cells as revealed by admittance spectroscopy and related methods, Applied Physics Letters, 100 (2012). http://dx.doi.org/10.1063/1.4729751
[43] O. Gunawan, T. Gokmen, C.W. Warren, J.D. Cohen, T.K. Todorov, D.A.R. Barkhouse, S. Bag, J. Tang, B. Shin, D.B. Mitzi, Electronic properties of the $Cu_2ZnSn(Se,S)_4$ absorber layer in solar cells as revealed by admittance spectroscopy and related methods, Appl. Phys. Lett. 100 (2012). https://doi.org/10.1063/1.4729751.
[44] T. Kirchartz, U. Rau, What Makes a Good Solar Cell?, Adv. Energy Mater. 8 (2018). https://doi.org/10.1002/aenm.201703385.
[45] Y.-R. Lin, V. Tunuguntla, S.-Y. Wei, W.-C. Chen, D. Wong, C.-H. Lai, L.-K. Liu, L.-C. Chen, K.-H. Chen, Bifacial sodium-incorporated treatments: Tailoring deep traps and enhancing carrier transport properties in Cu_2ZnSnS_4 solar cells, Nano Energy. 16 (2015) 438-445. https://doi.org/10.1016/j.nanoen.2015.07.022.
[46] M. Ishaq, S. Chen, U. Farooq, M. Azam, H. Deng, Z.-H. Su, Z.-H. Zheng, P. Fan, H.-S. Song, G.-X. Liang, High Open-Circuit Voltage in Full-Inorganic Sb_2S_3 Solar Cell via Modified Zn-Doped TiO_2 Electron Transport Layer, Sol. Rrl. 4 (2020). https://doi.org/10.1002/solr.202000551.
[47] L. Fan, Y. Ding, J. Luo, B. Shi, X. Yao, C. Wei, D. Zhang, G. Wang, Y. Sheng, Y. Chen, A. Hagfeldt, Y. Zhao, X. Zhang, Elucidating the role of chlorine in perovskite solar cells, J. Mater. Chem. A. 5 (2017) 7423-7432. https://doi.org/10.1039/c7ta00973a.

Supporting information

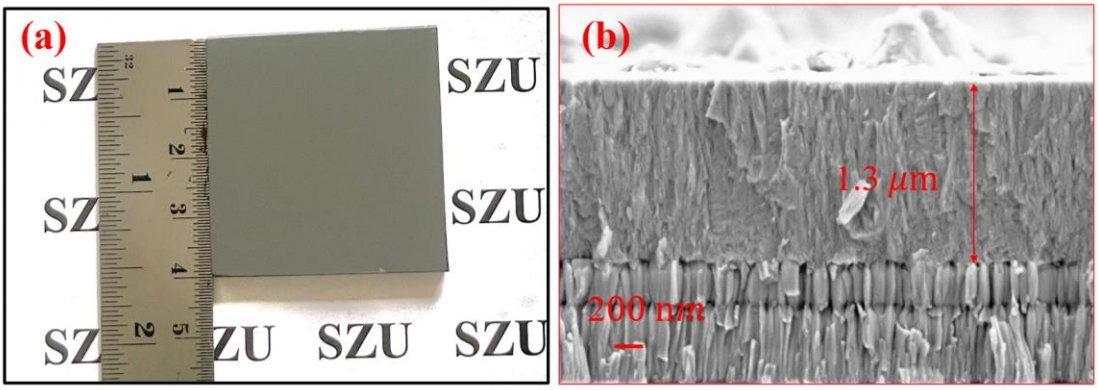

Figure S1. The 4 × 4 cm^2 precursor film photo (a) and SEM cross section images of the as-deposited CZTS thin-films (b)

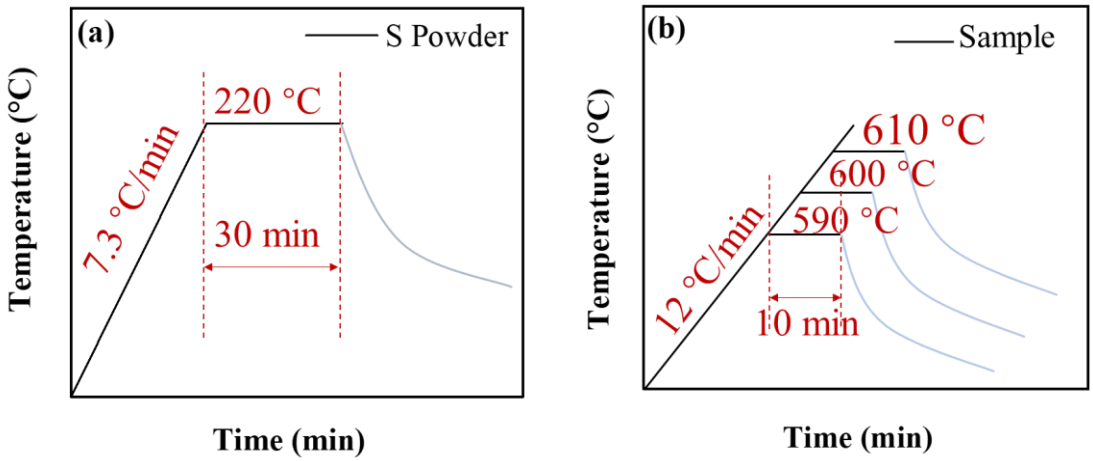

Figure S2. Temperature profile of the post-sulfurization treatment. (a) S powder Temperature Zone, (b) Sample zone.

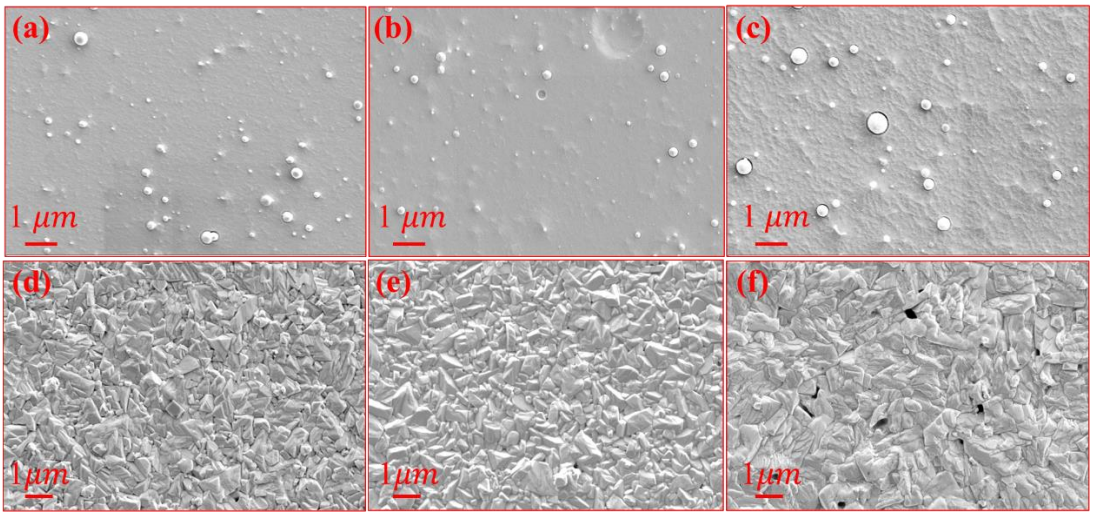

Figure S3. SEM of the precursors prepared under different laser energy, (a) 50 mJ, (b) 150 mJ (c) 250 mJ and the corresponding CZTS film morphology beneath, sulfurized at 600 °C.

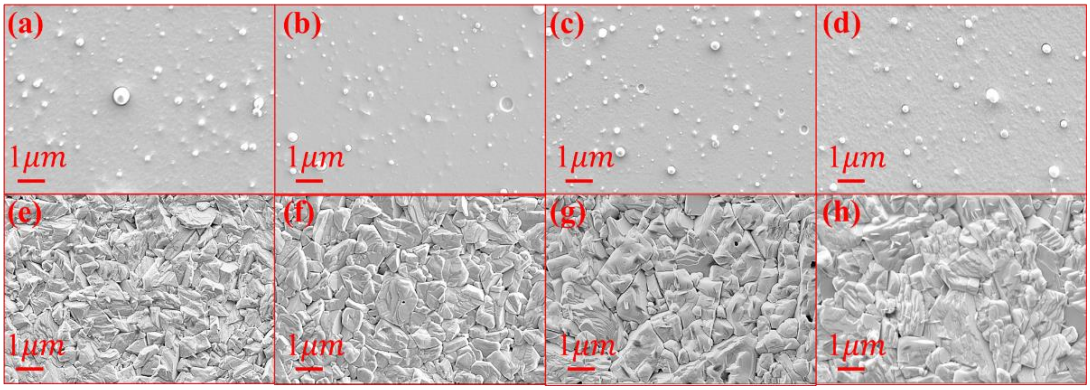

Figure S4. SEM of the precursors prepared with different substrate temperatures (a.100 °C, b. 200 °C, c. 300 °C, d. 400 °C) and the corresponding CZTS film morphology beneath, sulfurized at 600 ° C.

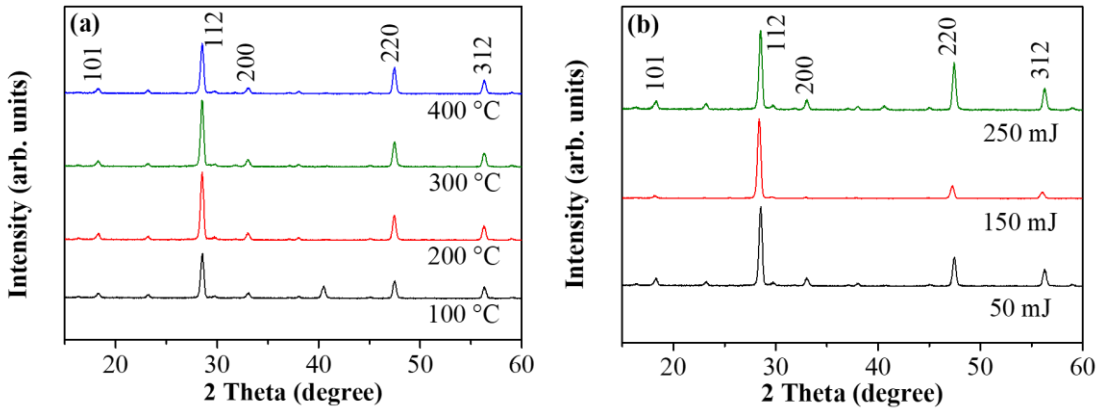

Figure S5. XRD of the CZTS thin films fabricated by (a)different substrate temperature and (b)different laser energy pulse.

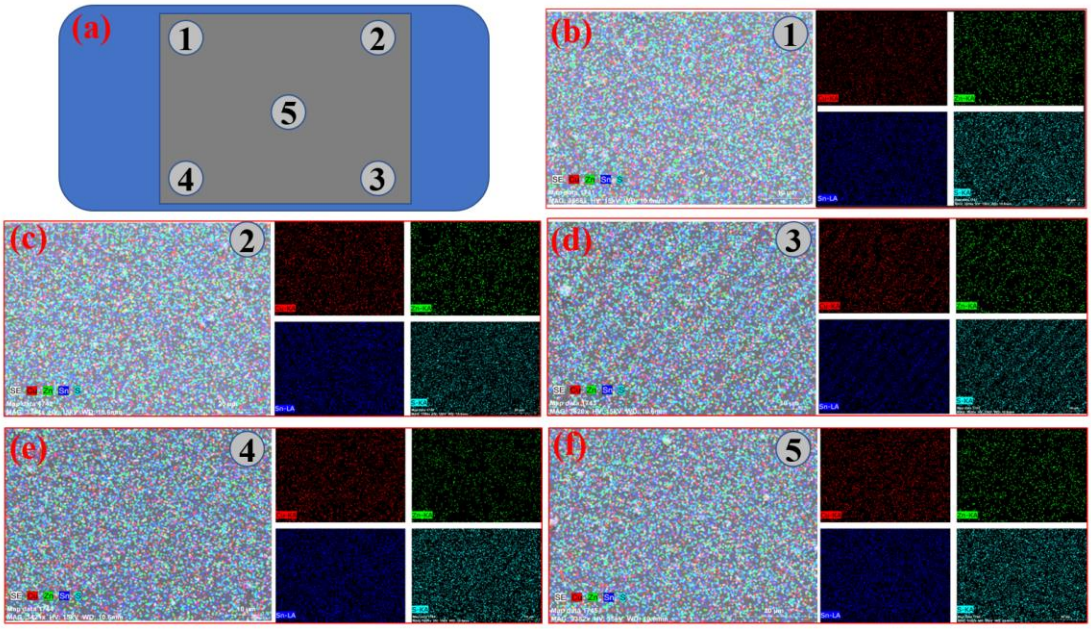

Figure S6. Chemical composition mapping of five point for as-deposition film fabricated by PLD. (a) Schematic diagram of the test location points on precursor. (b)-(f) Composition mapping of the corresponding points.

Table S1. The corresponding composition of five point for as-deposition film fabricated by PLD with the Cu, Zn, Sn and S elements.

Point	Cu(at%)	Zn(at%)	Sn(at%)	S(at%)	Cu/(Zn+Sn)	Zn/Sn	S/(Cu+Zn+Sn)
1	24.25	12.45	12.65	50.65	0.97	0.97	1.03
2	24.38	12.83	12.79	50.90	0.95	1.00	1.04
3	24.47	12.75	12.57	50.21	1.00	0.97	1.08
4	24.63	12.50	12.95	49.92	0.97	0.96	1.00
5	24.71	12.32	12.31	50.66	1.00	1.00	1.03